The EMBO Journal Vol.19 No.7 pp.1419–1431, 2000

Structure and mechanism of action of a novel phosphoglycerate mutase from *Bacillus stearothermophilus*

Mark J.Jedrzejas[1], Monica Chander[2], Peter Setlow[2] and Gunasekaran Krishnasamy

Department of Microbiology, University of Alabama at Birmingham, 933 19th Street South, Birmingham, AL 35294 and [2]Department of Biochemistry, University of Connecticut Health Center, Farmington, CT 06030, USA

[1]Corresponding author
e-mail: jedrzejas@uab.edu

Bacillus stearothermophilus **phosphoglycerate mutase (PGM), which interconverts 2- and 3-phosphoglyceric acid (PGA), does not require 2,3-diphosphoglyceric acid for activity. However, this enzyme does have an absolute and specific requirement for Mn^{2+} ions for catalysis. Here we report the crystal structure of this enzyme complexed with 3PGA and manganese ions to 1.9 Å resolution; this is the first crystal structure of a diphosphoglycerate-independent PGM to be determined. This information, plus the location of the two bound Mn^{2+} ions and the 3PGA have allowed formulation of a possible catalytic mechanism for this PGM. In this mechanism Mn^{2+} ions facilitate the transfer of the substrate's phosphate group to Ser62 to form a phosphoserine intermediate. In the subsequent phosphotransferase part of the reaction, the phosphate group is transferred from Ser62 to the O2 or O3 positions of the reoriented glycerate to yield the PGA product. Site-directed mutagenesis studies were used to confirm our mechanism and the involvement of specific enzyme residues in Mn^{2+} binding and catalysis.**

Keywords: *Bacillus stearothermophilus*/mechanism/phosphoglycerate mutase/spores/structure

Introduction

Phosphoglycerate mutase (PGM) plays an essential role in the pathways of both glycolysis and gluconeogenesis, where this enzyme interconverts 3-phosphoglyceric acid (3PGA) and 2-phosphoglyceric acid (2PGA). There are two different types of PGM, the cofactor-dependent PGMs (dPGMs) that require 2,3-diphosphoglyceric acid (DPG) for catalysis, in which this latter molecule participates as a phosphate donor, and the cofactor-independent PGMs (iPGMs) that do not require DPG. The dPGMs are the major and often the only PGM present in vertebrates (including humans), certain invertebrates, fungi and some bacteria, primarily Gram-negative ones such as *Escherichia coli*. These enzymes have a polypeptide of ~25 kDa, are invariably oligomeric, and their amino acid sequences are well conserved across species (Fothergill-Gilmore and Watson, 1989). The dPGMs are also evolutionarily related to a family of acid phosphatases (Schneider *et al*., 1993) and to fructose 2,6-bisphosphatase (Bazan and Fletterick, 1990). The iPGMs are the only or predominant PGM in higher plants, selected invertebrates, some algae and fungi, and many other bacteria, in particular Gram-positive bacteria including members of the spore-forming *Bacillus* and *Clostridium* species as well as closely related organisms that have lost the ability to form spores (Chander *et al*., 1998). These latter organisms include members of *Staphylococcus* and *Streptococcus* species, some of which are important human pathogens. Consequently, it is possible that iPGMs could be a target for rational design of a novel antibiotic. Interestingly, some bacteria have genes for both an iPGM and a dPGM, but only one enzyme comprises the great majority of these organisms' PGM activity (Fraser *et al*., 1999). In contrast to the dPGMs, the iPGMs function as monomers of ~60 kDa, and there is no significant sequence homology between these two types of enzymes, although the amino acid sequences of iPGMs have also been well conserved in evolution (Chander *et al*., 1999). In addition, iPGMs exhibit partial sequence homology to alkaline phosphatases, albeit only in an ~70 amino acid region corresponding to the metal-binding site of the alkaline phosphatases (Galperin *et al*., 1998). This suggests that iPGMs may be a divergent member of the alkaline phosphatase family. Taken together, these data indicate that the iPGMs and the dPGMs almost certainly have both different structures and catalytic mechanisms, and this latter point is further supported by the lack of inhibition of iPGMs by compounds such as vanadate that inhibit the dPGMs. However, while the structure and mechanism of the dPGMs are known in great detail, this information is generally lacking for the iPGMs.

The iPGMs from many Gram-positive bacteria, in particular the enzymes from the spore-forming *Bacillus* species and their close non-spore-forming relatives, have an additional unique feature in that these enzymes have an absolute and specific requirement for Mn^{2+} ions for their activity (Singh and Setlow, 1979; Watabe and Freese, 1979). As with other Mn^{2+}-dependent enzymes such as rat liver arginase (Kuhn *et al*., 1991; Kanyo *et al*., 1996) and brain glutamine synthetase (Monder, 1965), this Mn^{2+} dependence makes catalysis by the iPGMs from *Bacillus* species exquisitely sensitive to pH in the range of 6–8 (Kuhn *et al*., 1995). This pH dependence is extremely important in the regulation of iPGM activity during spore formation and spore germination in these organisms. During the sporulation process the developing spore or forespore becomes somewhat acidified, resulting in iPGM inhibition and accumulation of 3PGA. Subsequent forespore dehydration leads to complete inactivity of the dormant spore's iPGM and thus a stable pool of 3PGA in the dormant spore comprising 0.15–0.3% of spore dry weight. However, when spore germination is initiated, the spore rehydrates and excretes protons. These two processes

result in the restoration of iPGM activity, rapid metabolism of the spore's 3PGA depot and generation of ATP that is used for biosynthetic reactions in the early minutes of the germination process (Magill *et al*., 1994, 1996).

In order to gain insight into the reason(s) for the Mn^{2+}- and pH-dependence of the iPGMs from *Bacillus* species, as well as the structure and mechanism of this group of enzymes, we have undertaken the structural characterization of the iPGM from *Bacillus stearothermophilus*. In previous work, we overexpressed and purified the iPGM from this organism in both the native and selenomethionyl form and obtained crystals of both forms of the enzyme (Chander *et al*., 1999). In this work, we present a high-resolution X-ray crystal structure of this protein complexed with both its 3PGA substrate and Mn^{2+} ions. We have also mutated certain key residues that appear likely to be involved in either Mn^{2+} binding and/or catalysis, and have purified and measured the activity and the pH- and Mn^{2+}-dependence of the activity of these mutant proteins. Based on the results from all of these studies we have proposed a catalytic mechanism for this enzyme.

Results

Overall structure of Bacillus stearothermophilus iPGM

The crystal structure of the iPGM from *B.stearothermophilus* was solved at 1.90 Å resolution (Figure 1; Table I). The structure encompasses residues 3–510 of the 510 amino acids in the mature protein and also includes two Mn^{2+} ions, the 3PGA substrate and 180 ordered water molecules. The presence of two Mn^{2+} ions in the structure is consistent with Mn^{2+} binding studies with this enzyme in solution, and both Mn^{2+} ions appear essential for enzyme activity (P.Setlow, unpublished results). The structure of this iPGM is completely different from the structure of the *Saccharomyces cerevisiae* dPGM, which has also been determined by X-ray crystallography (Campbell *et al*., 1974; Rigden *et al*., 1998). Note that the translation-initiating Met1 residue of *B.stearothermophilus* iPGM is removed post-translationally, therefore the full-length, mature enzyme consists of residues Ser2 and Lys511. In addition, single residues at both the N- and C-termini, Ser2 and Lys511, are poorly ordered and are not included in the model. The electron density is of high quality, allowing for good definition of the model; the central buried core of the structure is especially well defined as judged by good electron density and low temperature factors in the final model. The most poorly defined parts of the structure are two loops, Ser299–Gly304 and Glu349–Glu355, which are in regions of the protein highly exposed to the solvent.

The iPGM adopts a compact, globular shape with two domains, A and B (Figures 1 and 2). Domain A contains residues Lys3–Ala71 and Thr316–Val510; domain B encompasses Leu79–Tyr305. The overall structure contains 17 α-helices (33.9% of all residues) and 16 β-strands (15.9% of all residues) (Figure 1B). The polypeptide chain begins in domain A, continues through domain B and ends in domain A. The two domains are similar in size with approximate dimensions of 24 × 35 × 31 Å. In domain A only one of the eight β-strands is antiparallel to the other seven parallel β-strands, while in domain B there are two parallel strands that are antiparallel to the remaining six parallel β-strands. In domain A there is one β/α/β unit (Gln328–Ile360) and in domain B there are four β/α/β units (Leu111–Gly140, Val144–Gly184, Thr212–Ile238 and Ala254–Thr296). These β-sheet structures are located in the core of each domain and are surrounded by helices of various lengths. There are eight and nine helices in domains A and B, respectively, and the helices vary in both their length and orientation. Helix Leu411–Lys435 is the longest one in domain A and helix Thr159–Gly175 is the longest one in domain B; both of these helices are exposed to the surface of the protein. The overall topology of the protein is shown in Figure 1 and like other glycolytic proteins the PGM structure can be described as α/β-type structure (Sternberg *et al*., 1981).

Domains A and B are bridged by two loops, 1 and 2, of seven (Gly72–Ser78) and 10 (Val306–Asn315) residues, respectively. The loops are separated by ~10 Å (backbone to backbone distance) and their orientation is stabilized by many hydrogen bonds. These include inter-loop hydrogen bonds formed between the backbone oxygen atoms of residues Asp314 and Lys309 in loop 2 and both the NH1 (2.94 Å) and NH2 (2.67 Å) nitrogen atoms of Arg73 and the NH1 nitrogen atom of Arg81 (2.92 Å) in loop 1. The A and B domains also interact through a hydrogen bond network, and these interactions are composed mainly of the following contacts: OD2 (Asp263)–NE2 (His 339) (3.13 Å); O (Gly120)–NE2 (Asn58) (2.84 Å); NE (Arg191)–OE1 (Glu335) (3.20 Å); O (Arg153)–O (Thr460) (2.82 Å); O (Gly152)–OG1 (Thr460) (2.78 Å); as well as a salt bridge OD1 (Asp192)–OE2 (Glu335) (2.58 Å). The connecting surface of domain A is convex whereas that of domain B is concave, allowing a complementary fit between the two domains, and a well defined cleft is present between the two domains. Although this cleft is not defined by any secondary structural motifs, both sides of the cleft are built from connecting loops between α-helices and β-strands. The cleft is highly solvent accessible and many of the ordered water molecules are found here (see below) as are the 3PGA substrate and two Mn^{2+} ions (Figures 1 and 3). The 3PGA substrate is oriented such that the phosphate is close to domain A with the carboxylate near domain B (Figure 1; Table II). The metal-binding sites are in a crevice formed by strands β1 and β14 of domain A. Out of 180 ordered water molecules in the overall structure, nearly 80 are in the cleft between domains A and B; the remaining water molecules are distributed on the surface of the protein.

The active site

The active site, defined as residues interacting with either the 3PGA or the Mn^{2+} ions, consists of 14 residues from both domains: Asp12, Ser62, Lys336, Asp403, His407, Asp444, His445 and His462 from domain A; and His123, Asp154, Arg185, Arg191, Arg261 and Arg264 from domain B (Figure 3A; Table II). Access to the active site is easy because it is located in the cleft between the two domains. In addition to the 3PGA substrate, the active site also contains two Mn^{2+} ions that are 4.80 Å apart; each Mn^{2+} ion has five coordinating ligands with distorted square pyramidal geometry, which is common for Mn^{2+} ions. The coordination sphere of Mn1 includes interactions with Asp403, His407 and His462 (average metal–ligand

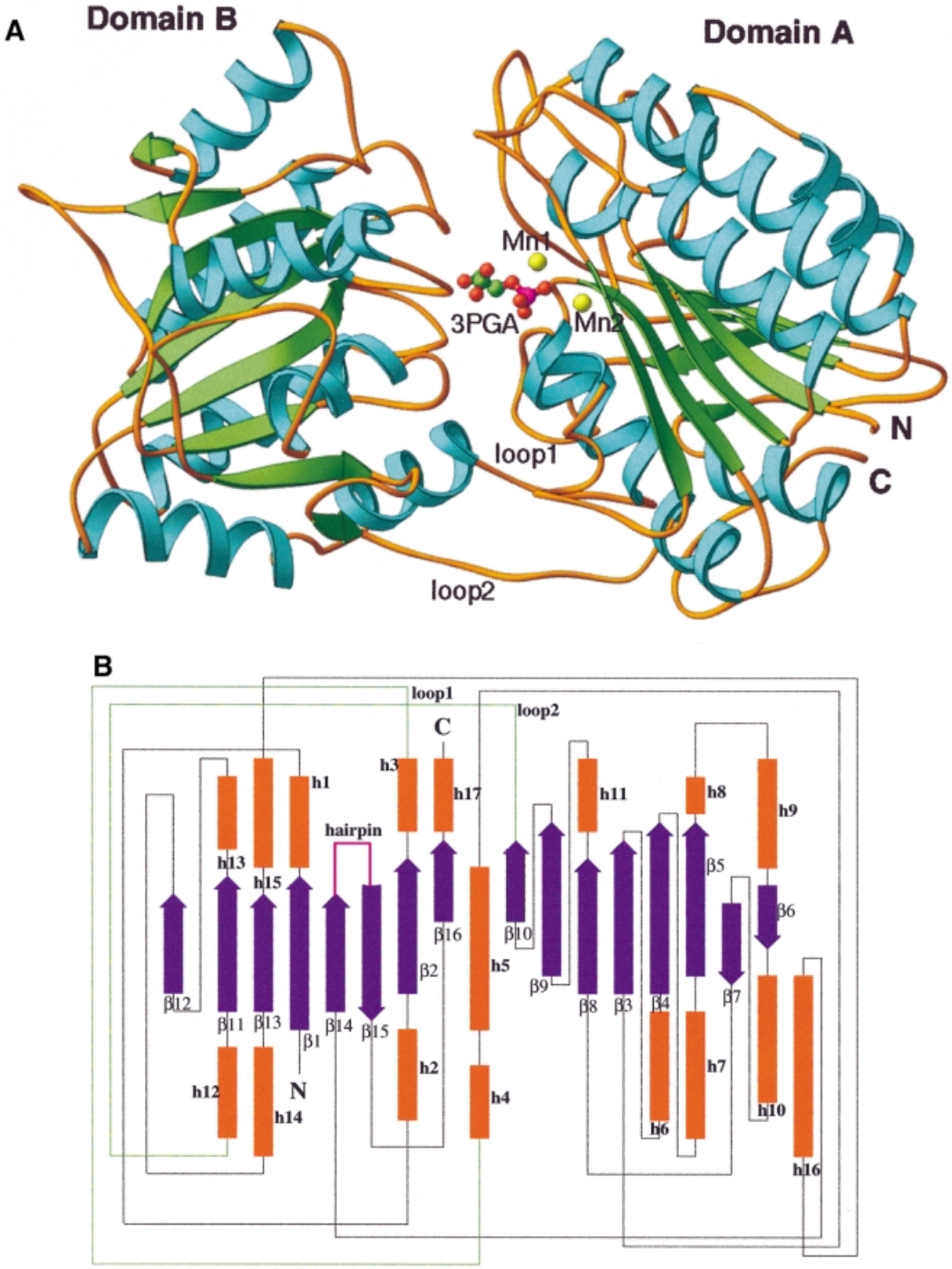

Fig. 1. (**A**) Ribbon drawing of *B.stearothermophilus* iPGM. The Mn^{2+} ions and the 3PGA substrate molecule are shown in a ball-and-stick fashion. (**B**) Topology diagram of *B.stearothermophilus* iPGM. The β-strands are shown as arrows and labeled with 'β'; the helices are represented as rectangles and labeled with 'h'. The locations of loop1, loop2 and the hairpin are also shown. The limits of the secondary structure elements are as follows: β1(6–11)-αh1(24–27)-αh2(31–39)-β2(42–45)-3_{10}h(49–52)-αh3(62–71)-αh4(78–87)-3_{10}h(91–93)-αh5(95–106)-β3(111–117)-αh6(126–138)-β4(144–150)-αh7(160–174)-β5(179–184)-αh8(185–188)-αh9(195–207)-αh10(216–225)-3_{10}h(230–232)-β7(236–238)-β8(254–257)-αh11(266–273)-β9(291–296)-β10(305–308)-αh12(317–323)-β11(328–333)-3_{10}h(334–336)-αh13(337–340)-β12(355–360)-3_{10}h(368–370)-αh14(376–389)-β13(394–399)-αh15(401–406)-αh16(411–434)-β14(438–442)-β15(467–471)-β16(481–483)-3_{10}h(484–486)-αh17(487–494).

distance of 2.12 Å) and with the phosphate oxygen atoms O1P and O3P (metal–ligand distance of 2.56 and 2.38 Å, respectively) (Figure 3; Table III). Ligands OD1 (Asp403), NE2 (His407), O1P and O3P are planar with Mn1, deviating from this plane only by 0.17 Å. The apex of the square pyramidal coordination geometry is occupied by NE2 (His462). The average angle between the ligands in the plane is 89.1°, whereas the angle between the apex and the in-plane ligands is 97.1°. Mn2 also has distorted square pyramidal coordination geometry defined by ligands Asp12 (bidentate interaction), Ser62, Asp444 and His445 (average metal–ligand distance of 2.26 Å) (Figure 3; Table III). The apex of this coordination is occupied by the OG oxygen atom of Ser62, and Mn2

Table I. Crystallographic analysis of *B.stearothermophilus* iPGM with 3PGA and Mn^{2+} ions

	Resolution (Å)	No. of unique reflections	Data coverage (outer shell) (%)	R_{sym}[a] (%)
Se-methionyl derivative				
λ1 = 0.9791 Å	2.0	45 244	89.4 (10.2)	11.4 (24.6)
λ2 = 0.9788 Å	2.0	44 950	88.6 (4.3)	11.1 (15.0)
λ3 = 0.9500 Å	2.0	48 009	92.9 (46.4)	8.3 (27.6)
Native	1.9	59 507	96.2 (85.1)	9.9 (23.3)

Refinement	Resolution range (Å)	Reflections (all)	Atoms modeled protein (water)	R_{cryst} /R_{free}[b] (outer shell)	r.m.s.[c]	
					Bond	Angle
	30.0–1.9	50 635	4186 (180)	20.71/24.70 (36.50/34.76)	0.007	1.3

[a]$R_{sym} = \Sigma I - <I>/\Sigma I$, where I is the intensity of an individual measurement and $<I>$ is the average intensity from multiple observations.
[b]$R_{cryst} = \Sigma\, |F_{obs} - F_{cal}|/\Sigma\, |F_{obs}$ (R_{free} was calculated with 10% of the reflections).
[c]Root-mean-square (r.m.s.) of bond lengths and angles are the deviations from ideal values; the r.m.s. deviation in *B*-factor is calculated between bonded atoms.

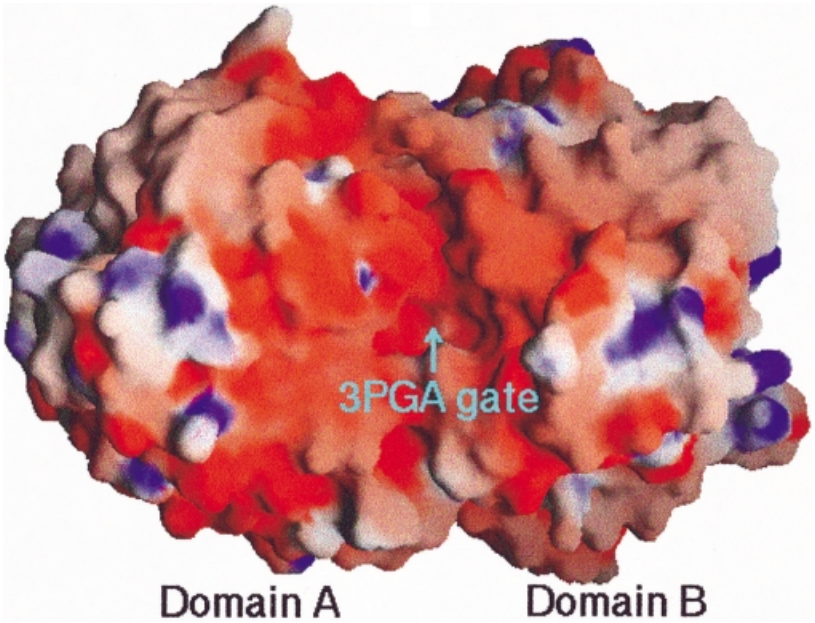

Fig. 2. Molecular surface of the whole *B.stearothermophilus* iPGM. The negative potential areas are represented in red and positive potential regions are in blue.

deviates only by 0.28 Å from the basal coordination plane. The average angle between in-plane ligands is 85.0° and between the apex and the in-plane ligands is 103.2° (Figure 3B; Table II) (Harding, 1999). As discussed below, the Mn^{2+} ions keep the active site residues in the appropriate orientation for tight binding of the phosphate group of the 3PGA substrate and also participate in the catalytic reaction. Consequently, the involvement of three histidine residues in the binding of the two Mn^{2+} ions thus explains the pH sensitivity of this enzyme's catalysis at low Mn^{2+} concentrations (Kuhn *et al.*, 1995) as well as the pH sensitivity of Mn^{2+} binding to the enzyme (P.Setlow, unpublished results).

The carboxyl end of the 3PGA substrate interacts with loops between β3 and h6, β4 and h7, β8 and h11, and with helix h8. The phosphate part of the substrate interacts with loops between β8 and h11, h8 and h9, the N-terminal loop of helix h13, the hairpin (via His445 and His462), and the N-terminus of helix h3 (Figure 1B). The carboxyl group of the substrate interacts in a bidentate fashion with Arg264 (average distance of 2.87 Å), whereas the hydroxyl group (O2) interacts with Asp154 (2.753 Å) and Arg185 (2.80 Å). There is an ordered water molecule in the active site, Wat17, which directly interacts with the O1b oxygen of the substrate carboxyl group (2.82 Å) and with the O1P ester oxygen atom of the phosphate group (3.39 Å). The position of this water molecule in close proximity to Mn1, as well as its interactions with the 3PGA substrate, suggests a direct involvement of this molecule in the catalytic reaction through its ionization while coordinated with Mn1 during the catalytic cycle (see below). Two oxygen atoms of the phosphate group (O2P and O4P) are hydrogen bonded with Arg261 in a bidentate fashion (average distance of 2.79 Å), and the O4P oxygen is also close to the backbone nitrogen atom of Ser62 (2.99 Å). Additionally, the O3P atom interacts with the side chain

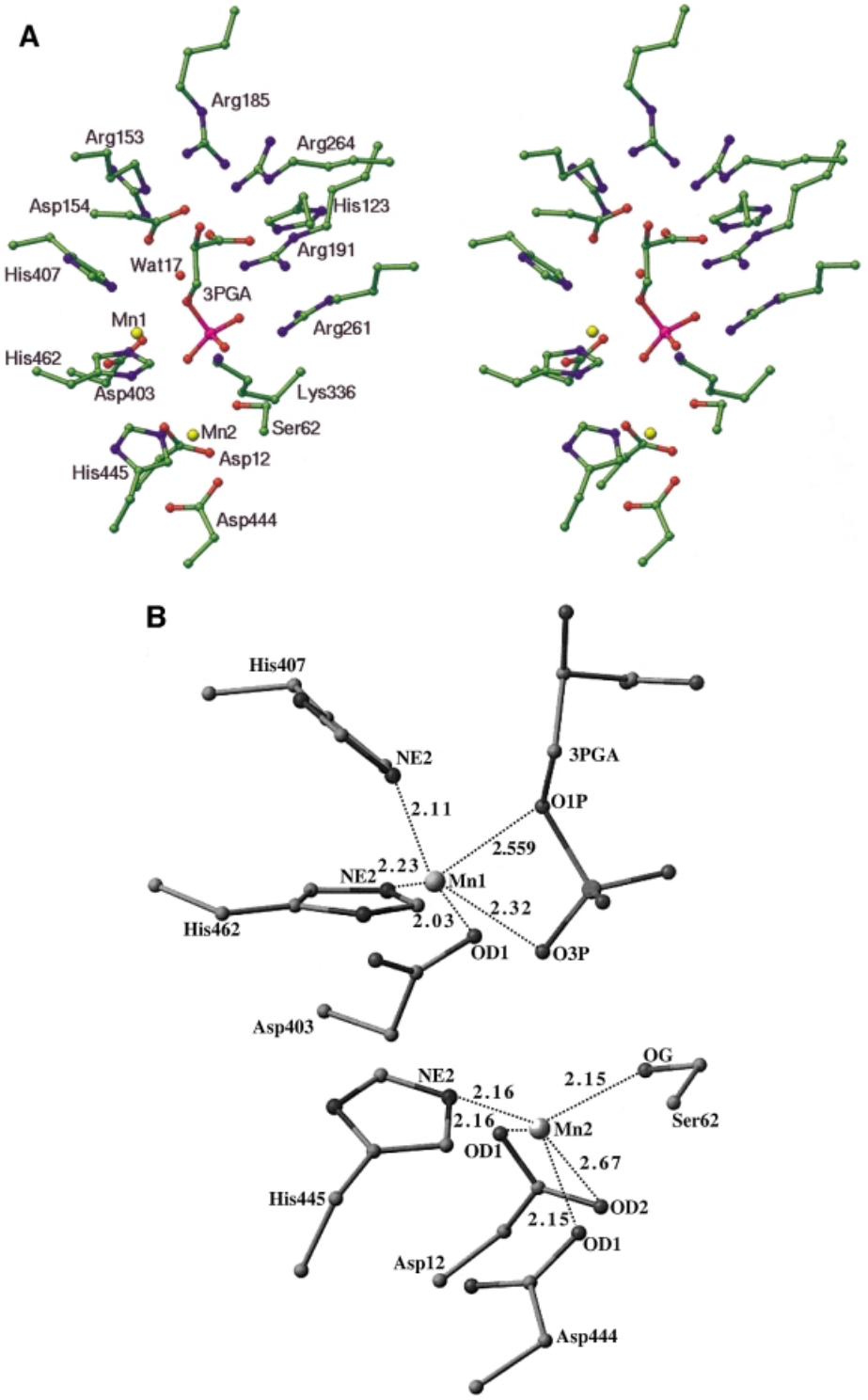

Fig. 3. (**A**) The interaction of active site residues with the 3PGA substrate and Mn^{2+} ions. A total of 14 residues constitute the active site of iPGM. These include residues interacting with Mn^{2+} ions and residues interacting with 3PGA. (**B**) Coordination sphere of Mn^{2+} ions. The coordination sphere of both Mn^{2+} ions is distorted square pyramidal. The atoms occupying the apex positions are NE2 of His462 for Mn1 and OG of Ser62 for Mn2.

oxygen of Ser62 with a distance of 2.79 Å and the distance from this oxygen of Ser62 to the phosphorus atom of 3PGA is 3.36 Å. The details of the interactions in the active site are provided in Tables II and III and Figure 3.

Residue Lys336 interacts with two Mn^{2+}-coordinated ligand atoms: the substrate's phosphate oxygen, O3P (Nz Lys336–O3P = 2.63 Å), and the OG atom of Ser62 (Nz Lys336–OG Ser62 = 2.62 Å). Residue His66 interacts with both Asp12 (OD2) and the backbone carbonyl oxygen of Ser62 to keep these residues in the desired orientation. Additionally, the one ordered water molecule in the active site interacts with the carboxyl oxygen O1b of the substrate (2.82 Å) and the ester oxygen O1P (3.39 Å).

Residues Ala443–Pro466 including active site residues

Table II. The non-bonding interactions in the active site of *B.stearothermophilus* iPGM

Atom (residue)	Atom (residue)	Distance (Å)
Substrate with protein		
O1a	NE2 (H123)	2.69
	NH1 (R191)	3.36
	NE (R254)	2.88
O1b	Wat17 (water)	2.82
	NH2 (R264)	2.86
	NE (R153)	3.17
O2	NE2 (H123)	3.13
	OD1 (D154)	2.75
	OD2 (D154)	3.01
	NH2 (R185)	2.80
	NH1 (R185)	3.16
O1P (ester)	Wat17	3.39
O2P	NH2 (R261)	2.79
	NH1 (R191)	3.11
O3P	OG (S62)	2.79
	Nz (K336)	2.63
O4P	NH1 (R261)	2.79
	N (S62)	2.99
P	OG (S62)	3.36
	Nz (K336)	3.22
Wat17 (water) with protein		
	NH2 (R153)	2.79
	OD2 (D403)	3.05
	SD (M404)	3.02
Protein with protein		
NH1 (R185)	OD2 (D154)	2.94
NH1 (R191)	OD2 (D263)	3.24
NE (R261)	OD1 (D263)	2.99
NH2 (R261)	OD2 (D263)	2.85
N2 (K336)	OG (S62)	2.62
NE2 (H339)	NH2 (R261)	3.16
NE2 (H339)	OD2 (D263)	3.13
ND1 (H407)	O (T460)	2.60
ND1 (H445)	O (G446)	2.93
ND1 (H462)	O (G60)	2.76

Table III. Metal coordination in the active site of *B.stearothermophilus* iPGM with 3PGA and Mn^{2+} ions

Metal	Ligand (residue)	Distance (Å)	Ligand–metal–ligand angle (°)			
			H407	H462	O1P	O3P
Mn1	OD1 (D403)	2.03	105.2	102.1	163.2	98.5
	NE2 (H407)	2.11		102.0	87.0	145.0
	NE2 (H462)	2.23			86.7	97.7
	O1P (3PGA)	2.56				65.9
	O3P (3PGA)	2.32				
			OD2 D12	S62	D444	D445
Mn2	OD1 (D12)	2.16	53.1	110.8	116.0	154.1
	OD2 (D12)	2.67		86.0	73.6	154.1
	OG (S62)	2.15			96.3	119.9
	OD1 (D444)	2.15				102.6
	NE2 (H445)	2.16				
Mn1	Mn2	4.78				

Asp444, His445 and His462 form a 24 amino acid hairpin that folds to bring these residues into the active site. The hydrogen bond interactions between the backbones of Val451 and Gln459 (2.89 Å) and Thr453 and Lys457 (2.73 Å) assist in hairpin folding, and Pro454 forms a type-I β-turn that also assists in hairpin folding. The hydrogen bonds between the ND1 nitrogen atom of His462 and the backbone oxygen of Gly60 (2.76 Å), and the ND1 atom of His407 and the backbone oxygen of Thr460 (2.60 Å), orient the histidine residues for proper coordination with the Mn^{2+} ions. Residues His407 and His462 are nearly coplanar whereas residues His462 and His445 are in a parallel clapping hand orientation. Finally, OG of Ser62 interacts with the substrate's phosphorus atom (3.36 Å), which is suggestive of the involvement of this residue in the catalytic mechanism. Residue Pro55, which is in a loop between strand β2 and helix h3, is part of a type-I β-turn that assists in placing Ser62 in the proper orientation to allow for coordination with Mn2.

Site-directed mutagenesis of key residues

Based on the structure of the active site of this enzyme as discussed above, in particular the interactions of the 3PGA and the two Mn^{2+} ions with the protein, a number of amino acid residues appeared likely to be of major importance in enzyme catalysis. Consequently, residues Asp12, Ser62, His66, His123, Arg261, His407, His445 and His462 (Figure 3) were mutagenized to establish definitively both their role and their importance in catalysis. Mutagenized proteins were obtained and partially purified as described in Materials and methods, and all mutant enzymes were fully soluble and behaved as did the wild-type protein during purification. However, mutant proteins D12N, S62A, R261L and H407N exhibited no detectable PGM activity at any pH or Mn^{2+} concentration tested, while three variants (H66N, H123N, H462N) retained only between 0.3 and 3% of maximum catalytic activity and one protein (H445N) retained ~20% of maximum activity (Table IV). This latter protein was also interesting in that at least at pH 7 and 8 this variant required significantly higher concentrations of Mn^{2+} for high activity than did the wild-type or other mutant proteins (Table IV). This finding is consistent with the important role of His462 in Mn^{2+} binding. In addition to mutants with altered active site residues, several other variants were constructed with changes in His residues that are not in the active site but are conserved in iPGMs (Figure 4). These changes included: H42N, H112N, H125N, H128N, H147N and H297N. In contrast to the almost complete abolition of activity by alteration of residues in the active site, variants with an alteration of a conserved but non-active site residue retained at least 20% of maximum activity and in several cases exhibited increased activity (Table IV; data not shown). In addition, the activity of these variants exhibited responses to changes in pH and Mn^{2+} concentration similar to those of the wild-type enzyme (Table IV; data not shown).

Discussion

Sequence similarities

Comparison of amino acid sequences of known iPGMs from *Bacillus* and *Clostridium* species (Figure 4), as well as their relatively close but non-sporulating relatives (data not shown), shows a very high degree of sequence homology between these proteins, and all residues in the active site of the *B.stearothermophilus* iPGM are completely conserved (Figure 4, residues marked with an asterisk; data not shown). Comparison of the amino acid sequences of iPGMs from spore formers with those of iPGMs from *E.coli* (Sofia *et al.*, 1994) and maize (Grana

Table IV. Properties of wild-type and mutant *B.stearothermophilus* iPGMs[a]

Protein analyzed	Specific activity (% of WT)	Free Mn^{2+} (μM)	Activity at various pHs and Mn^{2+} concentrations (% of maximum activity)		
			pH 6	pH 7	pH 8
Wild type	100%	4	<0.1	4	28
		10	<0.1	9	31
		100	1	12	88
		1 mM	2	22	100
D12N	<0.1				
H42N	91	4	<0.1	9	37
		10	<0.1	12	77
		100	<1	20	89
	1 mM	2	25	100	
S62A	<0.1				
H66N	2	4	<0.1	<0.1	13
		10	<0.1	0.1	19
		100	<0.1	4	57
		1 mM	1	13	100
H123N	3	4	<1	<0.1	40
		10	<1	1	47
		100	2	16	72
		1 mM	17	82	100
H125N	67	4	<0.1	16	65
		10	<0.1	19	73
		100	2	24	79
		1 mM	3	87	100
H128N	20	4	<0.1	5	55
		10	<0.1	8	59
		100	<1	12	77
		1 mM	2	16	100
H42N-H128N	8	4	<0.1	5	48
		10	<0.1	10	50
		100	1	20	60
		1 mM	3	127	100
R261L	<0.1				
H407N	<0.1				
H445N	18	4	<0.1	<0.1	0.3
		10	<0.1	<0.1	0.8
		100	<1	4	39
		1 mM	5	11	100
H462N	0.3				

[a]iPGMs were partially purified and assayed as described in Materials and methods. All specific activities are reported compared with the maximum activity of either the wild-type enzyme or the protein in question at pH 8 and 1 mM free Mn^{2+}.

et al., 1992) again reveals significant homology, and again the active site residues in *B.stearothermophilus* iPGM are strictly conserved (Figure 4, residues marked with an asterisk). In addition, residues Gly60, His66 and Thr460, which influence the orientation of the Mn^{2+}-binding residues by hydrogen bond formation, are also strictly conserved throughout all iPGMs.

In addition to good sequence conservation among iPGMs, limited sequence homology has previously been noted between iPGMs and *E.coli* alkaline phosphatase (AP), but only over a stretch of ~70 residues. Strikingly, the metal-binding residues of iPGMs are conserved in AP, and these residues are also conserved among all APs known (Galperin *et al*., 1998). The limited sequence conservation of the residues responsible for metal binding in APs and iPGMs suggested that there might also be some structural similarities between these two proteins. However, structural similarity comparisons (DALI algorithm; Holm and Sander, 1994) of our iPGM structure with structures in the Protein Data Bank (PDB) gave only a low and insignificant structural similarity to *E.coli* AP. Both iPGM and AP are α/β proteins, although AP is a homodimer with one independent active site per monomer. The AP structure also consists of a central β-sheet surrounded by helices (Sowadski *et al*., 1985).

The absolute and specific requirement for Mn^{2+} ions for activity of the iPGMs of *Bacillus* species (Chander *et al*., 1998), the detection of Mn^{2+} ions in *E.coli* iPGM by electron paramagnetic resonance spectroscopy (Fraser *et al*., 1999) and the identity between the metal-binding residues of iPGMs and those of AP strongly indicate that all iPGMs are metalloenzymes, as has been suggested previously (Johnson and Price, 1988; Smith *et al*., 1988), most likely with Mn^{2+} ions in their active site.

General properties of the iPGM active site

dPGMs catalyze an intermolecular phosphate transfer involving a phosphoenzyme intermediate (Nairn *et al*., 1995), and this intermediate has been identified in *S.cerevisiae* dPGM as phosphoHis8 (Rose, 1971). A second histidine residue in the active site, His181, appears to be a proton donor/acceptor for the negatively charged bridged oxygen atom of the phosphate group of the phosphoenzyme intermediate, and the essential role of both histidine residues in the yeast enzyme has been

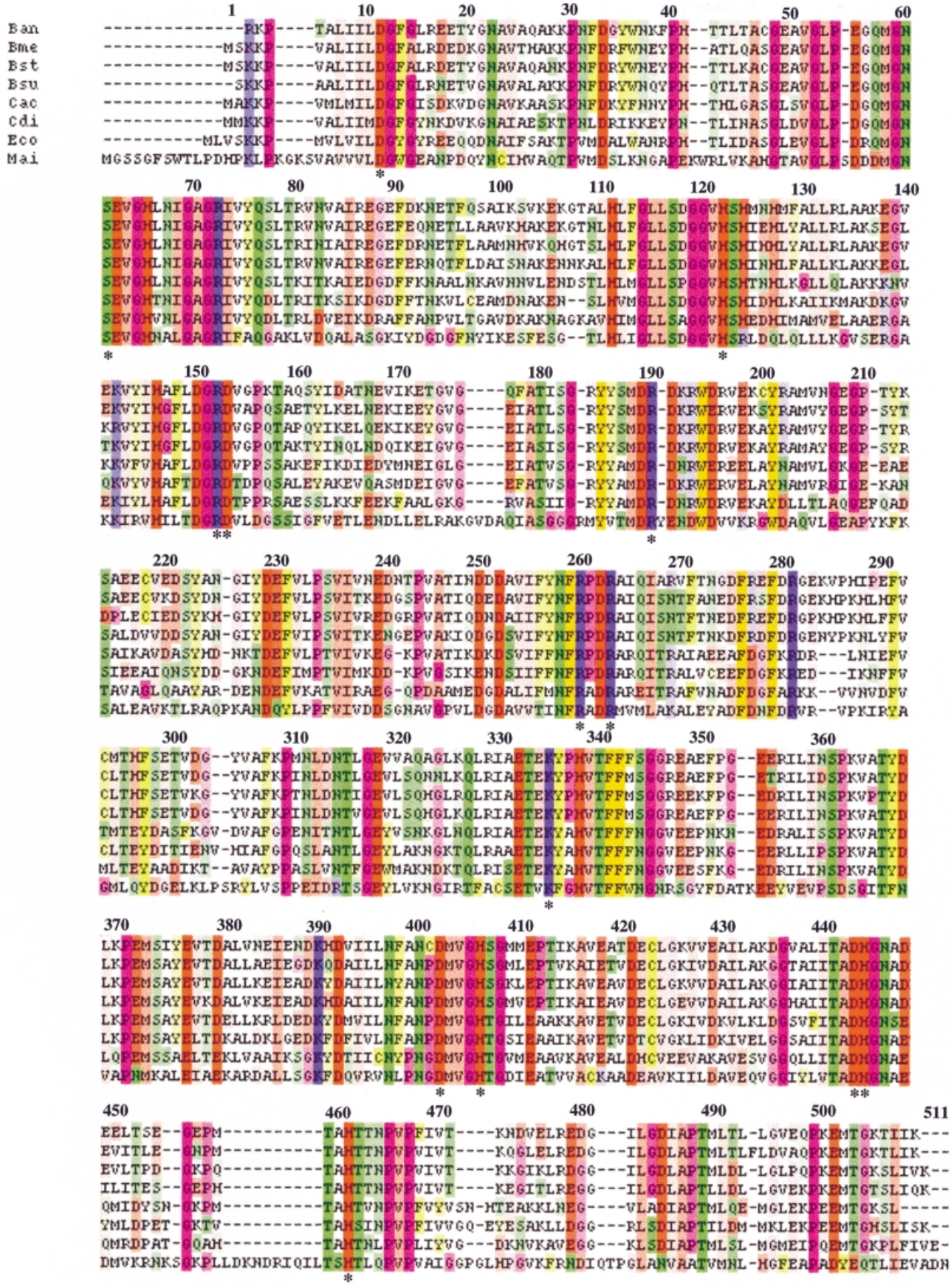
Ban
Bme
Bst
Bsu
Cac
Cdi
Eco
Mai

confirmed by site-directed mutagenesis (White and Fothergill-Gilmore, 1992; White *et al*., 1993).

The mechanism of iPGM catalysis has been studied with wheat germ iPGM using a variety of techniques (Breathnach and Knowles, 1977; Blatter and Knowles, 1980). These studies indicate that iPGM catalyzes an intramolecular phosphate transfer (Britton *et al*., 1971; Gatehouse and Knowles, 1977), with phosphoryl migration most likely to involve the formation of a phosphoenzyme intermediate, with the phosphate being either covalently or non-covalently bound to the enzyme. However, such a phosphoenzyme intermediate has not yet been identified for any iPGM. The possibility of a tightly, but non-covalently bound metaphosphate in the active site as an intermediate in the reaction has also not been completely excluded. However, the high reactivity of such a phosphate moiety with water strongly suggests that such an intermediate is unlikely.

Catalytic mechanism

Given the information regarding the structure of the active site in *B.stearothermophilus* iPGM we propose that the interconversion of 3- and 2PGA catalyzed by iPGM proceeds via the formation of a phosphoenzyme intermediate on Ser62 (Figure 5). Upon 3PGA binding the OH^- derived from the ordered water molecule in the active site, Wat17 (see below), is removed from the square pyramidal coordination sphere of Mn1 and replaced by the ester oxygen atom (O1P) of 3PGA. The hydroxyl group of Ser62 undergoes polarization, which is induced either by Mn2 or by the nearby Lys336 (2.623 Å), and is likely to transfer its hydrogen atom to Lys336 or to the solvent. The enzyme reaction is initiated by the attack of the oxygen atom of Ser62, which coordinates to Mn2, on the phosphorus atom of the 3PGA substrate. This removes the phosphate from the glycerate (which remains tightly bound to the enzyme) and forms phosphoSer62 (Figure 5), while the newly formed negatively charged oxygen group of the glycerate, O3, coordinates with Mn1. During this process the distorted square pyramidal coordinations of both Mn1 and Mn2 are maintained as are the substrate bidentate interactions with Arg261 and Arg264. Ser62 is likely to stay coordinated to Mn2 during the whole process. The two Mn^{2+} ions are also likely to be bridged through the OG oxygen of the phosphoSer62 intermediate and both the phosphorus atom and the O3P oxygen atom of the phosphate group (Figure 5B). Asp154 is now in a favorable position to remove a proton from the hydroxyl group at C2 of the glycerate (O2–OD1 Asp154 = 2.75 Å; C2–O2–OD1 Asp154 = 108.6°) (Figure 3A; Table II). This is followed by the repositioning of the glycerate about the Mn1–O1P bond as well as other small changes in the geometry of the glycerate bringing the oxygen group, O2, near the phosphorus atom of phosphoSer62. The flexibility of the Arg191 and Arg261 side chains should allow for small movements in these residues that in turn can allow substrate movement in the enzyme's active site. The carboxyl end of the glycerate is stabilized by Arg191 and Arg261 during and after rotation about the metal–O1P bond as shown in Figure 5. This is then followed by nucleophilic attack of the O2 oxygen atom on the phosphorus atom from the direction of the previous O1P ester oxygen of 3PGA and the transfer of the phosphate group from Ser62 to the O2 atom of the glycerate. This concludes the overall reaction and Ser62 still maintains its coordination with Mn2 and the coordination of both Mn^{2+} ions is preserved. Finally, the water molecule present in the active site, Wat17, moves towards Mn1, undergoes ionization/polarization and the resultant OH^- replaces the 2PGA's hydroxyl oxygen (O3)

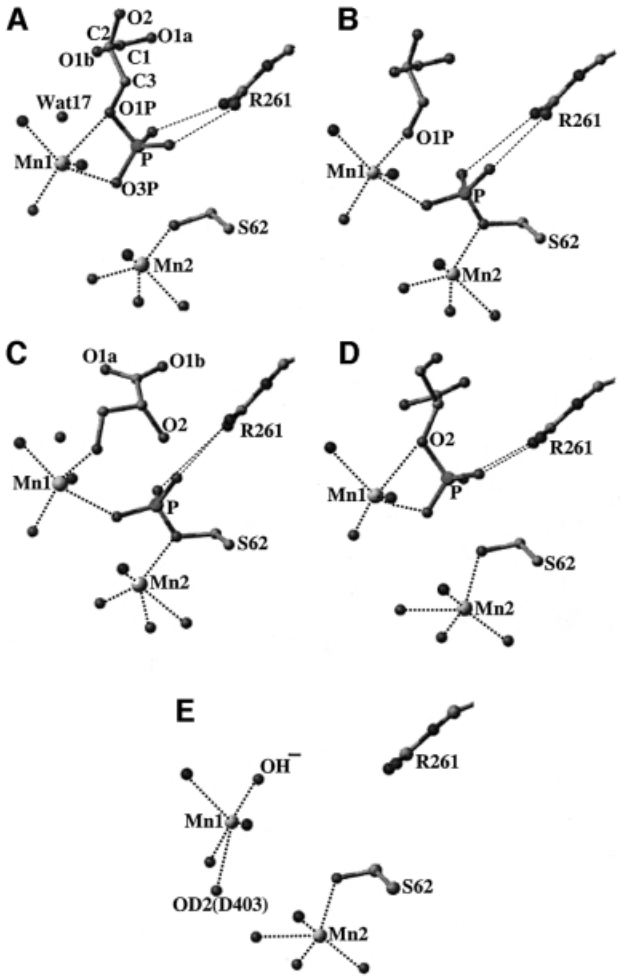

Fig. 5. The mechanism of phosphate group transfer from 3PGA to 2PGA by *B.stearothermophilus* iPGM. The major intermediates in the proposed catalytic mechanism are described in the text and are depicted as follows: (**A**) binding of 3PGA in the active site (based on the X-ray coordinates); (**B**) formation of a phosphoserine intermediate; (**C**) repositioning of the glycerate; (**D**) formation of 2PGA (based on the coordinates of the 2PGA–enzyme complex model); and (**E**) dissociation of the 2PGA–enzyme complex.

Fig. 4. Comparison of the deduced amino acid sequences of iPGMs. The abbreviations used are: Ban, *Bacillus anthracis* (obtained from The Institute for Genome Research website at www.tigr.org); Bme, *Bacillus megaterium*; Bst, *B.stearothermophilus*; Bsu, *Bacillus subtilis*; Cac, *Clostridium acetobutylicum* (obtained from www.ncbi.nlm.nih.gov/BLAST/unfinishedgenome.html); Cdi, *Clostridium difficile* (obtained from The Sanger Center website at www.sanger.ac.uk); Eco, *E.coli* (Sofia *et al*., 1994); and Mai, maize. Conserved residues in the sequences are colored according to residue properties: red, positively charged; blue, negatively charged; pink, hydrophobic. Residues marked with an asterisk are active site residues conserved in all iPGMs.

in coordination with Mn1 and displaces the 2PGA product. The proton from the ionized water molecule neutralizes the charge on the O3 of the 2PGA product in the process. The hydroxide ion remains coordinated to Mn1 until another substrate molecule binds in the enzyme's active site and replaces the OH^- in the Mn1 coordination sphere. The leaving OH^- ligand might then be neutralized to create a water molecule by gaining a proton, which is likely to be from Arg153 or from the bulk solvent. In this reaction mechanism, the absolute configuration about the phosphorus atom is retained as indicated by previous work (Breathnach and Knowles, 1977).

In order to confirm the above mechanism we modeled the 2PGA product of the reaction in the iPGM active site and energetically refined this structure as described in Materials and methods (Figure 5D). The active site of iPGM easily accommodates 2PGA without any major structural changes in the coordinates of protein residues or Mn^{2+} ions. The major interactions of protein residues with 3PGA in the active site are also seen with 2PGA, and the coordination spheres of the Mn^{2+} ions are again intact and distorted square pyramidal. The modeled 2PGA also coordinates with Arg261 (phosphate group) and Arg264 (carboxylate group) in a bidentate fashion. The only small changes that were observed between 2PGA and 3PGA in their active site interactions were in the interactions with the glycerate part of the substrate, while the phosphate binding and the Mn^{2+} environment is unchanged. Thus, the iPGM active site can easily accommodate either 3PGA or 2PGA, and these studies also explicitly show that the interconversion of 2PGA and 3PGA can proceed in either direction, as expected. However, once the phosphoenzyme has formed, the transfer of phosphate back to the position it came from, i.e. from 2PGA and then back to 2PGA, seems unlikely. This kind of repositioning would involve breaking the interaction between O2 or O3 of the substrate with Mn1, which is likely to require a significant amount of energy to break such a bond. Therefore, the only favorable repositioning of the glycerate is to bring the alternative oxygen atom close to the phosphorus atom without breaking the interactions with Mn1.

When the 3PGA/2PGA substrate is dephosphorylated by Ser62, the previously ester oxygen O3 of the 3PGA substrate or O2 of the 2PGA substrate enters the coordination sphere of Mn1. As a consequence, this oxygen atom loses its ability to interact with the phosphate group as it would require removing this oxygen from coordination with Mn1. However, another oxygen atom of the resultant glycerate (O2 for 3PGA or O3 for 2PGA) is available for interactions with the phosphate group and for nucleophilic attack on the phosphorus atom of the phosphoenzyme as described above. The maintenance of strong interactions of one of the glycerate substrate's oxygen atoms with Mn1 as well as interaction of the glycerate's carboxyl group with Arg264 allows for the reorientation of glycerate in the active site. After this reorientation of the glycerate, its oxygen atom that does not coordinate with Mn1 (O2 for 3PGA or O3 for 2PGA) is in the proper position to facilitate the removal of the phosphate group from Ser62 and for the formation of either 2PGA or 3PGA.

Although the mechanism in which Ser62 is the enzyme's phosphate acceptor seems most likely, it is difficult to eliminate His462 as a phosphoacceptor purely on structural grounds. His462 is coordinated with Mn1, and if this residue were to be phosphorylated, the phosphohistidine would be stabilized only by Mn1, and Mn2 would probably not be involved in the catalysis. After reorientation of the active site, the hydroxyl oxygen at C2 of the 3PGA could come close to the phosphohistidine at His462, but this would only take place with introduction of a significant amount of strain. More definitively, mutagenesis of H462 to Asn did not completely abolish enzyme activity, as the H462N mutant retained 0.3% activity (Table IV). In contrast, the S62A mutant lost all detectable activity (Table IV), as would be expected if this residue functioned as a phosphoacceptor in catalysis (Stec *et al*., 1998).

Further analysis of site-directed mutants

Comparison of the primary sequences of iPGMs from bacterial and plant sources (Figure 4) shows that the active site residues interacting with the substrate and the two Mn^{2+} ions are completely conserved. The importance of these residues in enzyme catalysis was confirmed by analysis of site-directed mutants (Table IV). Most mutations of active site residues resulted in an enzyme with greatly diminished activity. The S62A mutation would alter this residue's interaction with both the 3PGA phosphate and Mn2, and would compromise the enzyme's ability to form the hypothetical phosphoserine intermediate essential for catalysis. The R261L mutation would destroy this residue's bidentate interaction with the 3PGA phosphate, and this change would be likely to result in misplacement of this latter group for catalysis. The H123N mutation would alter the positioning of the glycerate part of the substrate, as His123 interacts with the carboxyl group oxygen atom O1a of the glycerate. Misalignment of the glycerate would in turn affect its ability to orient itself properly for catalysis, although this mutant enzyme retains 3% of wild-type activity. Finally, mutations D12N, H407N and H462N directly alter the interactions of the protein with Mn1 and Mn2. Since the proper orientation and coordination of these ions are crucial for enzyme catalysis, it is not surprising that these mutations abolish at least 99.7% of enzyme activity. The one mutation of an active site residue that does not eliminate essentially all enzyme activity is H445N, which retains 18% of wild-type activity. However, this mutant protein requires much higher concentrations of Mn^{2+} than the wild-type enzyme for equivalent activity. His445 is involved in coordination with Mn2 (Figure 3B) and mutation of this residue to Asn would be likely to distort this coordination and thus the enzyme's binding of Mn^{2+}. This change in Mn2 coordination did negatively affect enzyme catalysis but not completely, as this variant retains significant activity at high concentrations of Mn^{2+}.

Even though H66 is not directly involved in Mn^{2+} binding or interaction with the substrate, the H66N mutant also retained very little activity. Analysis of the structural data indicates that His66 interacts with Asp12 (OD2, 3.38 Å), Ser62 (O, 2.89 Å) and Asp444 (OD1, 2.98 Å). These three residues coordinate with Mn2, which is thought to be involved in catalysis through interaction with the substrate's phosphate group and also orienting Mn2 properly for catalysis. Interaction of His66 with Ser62 is also essential for proper positioning of this latter

residue for coordination with the phosphate group, which is again essential for catalysis. Consequently, changing His66 to Asn would be expected to have a detrimental influence on the active site environment, and this change does indeed essentially abolish catalytic activity.

While His128 is not in the active site, it is in close proximity to active site residue His123. His128 also interacts with Asn83 (OD1) from the h4 helix (2.92 Å), which connects through the inter-domain loop1 with the h3 helix, which has the catalytic Ser62 at its end; the proximity of His128 to Asn83 and the latter's proximity to the catalytic residue, His123, are likely to play a role in the positioning of active site residues Ser62 and His123. These effects are likely to be the reason that the H128N mutation results in loss of ~80% of enzyme activity. Additionally, mutation of the surface-exposed residue His125 to Asn (H125N) decreases PGM activity slightly, which is also likely to be due to the proximity of this residue to the active site His123.

Ser62 is the very first residue of helix h3 that is connected on one side by a small loop with β-strand β2 and with helix h4 by the inter-domain connecting loop1 with Asn83. Strand β2 is mostly exposed to the protein surface and its position is primarily stabilized by a stacking interaction between His42 at the end of the β2 strand and Trp37 at the end of the connecting helix h2, and by a hydrogen bond interaction with the same residue (ND1 His42–O Trp37 = 2.51 Å) (Figure 1B). The H42N mutation has almost no effect on the activity of the enzyme, presumably because of the at most minimal misplacement of Ser62. However, the double mutation H42N/H128N reduces enzyme activity >90%; presumably this is due to the combined effects of small changes in the positioning of the active site residues discussed above, Ser62 and His123. Mutation of other conserved His residues of iPGM not in the active site, H112N, H147N and H297N, resulted in no major decrease in enzyme activity (data not shown). Mutation of two conserved histidine residues in the active site of castor plant iPGM, His123 and His461 (*B.stearothermophilus* numbering scheme), also gave an inactive enzyme (Huang and Dennis, 1995), suggesting that the conclusions about the catalytic mechanism of *B.stearothermophilus* iPGM that can be drawn from our studies can also be extended to all iPGMs.

Conclusions

The active site of *B.stearothermophilus* iPGM has two Mn^{2+} ions and the enzyme utilizing the formation of a proposed phosphoenzyme intermediate in the process of catalysis. The catalytic mechanism of this enzyme is proposed to proceed with formation of a phosphoenzyme intermediate on a serine residue in the active site. Mn^{2+} ions play an essential role in this reaction, as these ions are involved in essentially all steps of the reaction. This essential role of the two Mn^{2+} ions results in the exquisite pH dependence of the reaction, as three His residues are involved in coordinating the enzyme's two Mn^{2+} ions. This pH sensitivity of iPGMs, in particular for the enzymes from spore formers, is essential for the accumulation of a depot of 3PGA in sporulation, as well as 3PGA catabolism and thus ATP production early in spore germination. Finally, the metabolic importance of iPGMs for some bacteria, in particular Gram-positive bacteria, and the apparent absence of iPGMs in vertebrates make this class of enzyme an ideal target for novel antibacterial drugs (Carreras *et al*., 1982).

Materials and methods

Generation of mutant clones, overexpression and partial purification of mutant proteins

Plasmid pPS2712, containing the 1.6 kb *pgm* gene from *B.stearothermophilus*, was used as the template for all mutagenesis reactions. Single base mutations were generated using a Transformer site-directed mutagenesis kit (Clontech) according to the manufacturer's instructions. The phosphorylated primers (with regions having changes from the wild-type sequence underlined) were: Snco (5′-GAGTGCACCATGGGC-GGTGTGAAAT-3′), used to change the unique *Nde*I site to *Nco*I in the multiple cloning site to facilitate subsequent isolation of mutants; D12N (5′-GCGCTCATCATTTTAAACGGATTTGCGC-3′), used to change Asp12 to Asn; S62A (5′-GGGCAACGCGGAAGTCGGCC-3′), used to change Ser62 to Ala; H66N (5′-GGAAGTCGGCAATCTCAAC-3′), used to change His66 to Asn; H123N (5′-GGGGTCAACAGGCCGG-CCATATTC-3′), used to change His123 to Asn; H128N (5′-CGATA-TTCACAATTTGTACGCCCTCTTGCGC-3′), used to change His128 to Asn; R261L (5′-CGCGATTATCTTCTATAATTTCCTCCCTGACCG-GG-3′), used to change Arg261 to Leu; H407N (5′-GGTCGG-CAATTCGGGCAAGC-3′), used to change His407 to Asn; H445N (5′-CGCCGACAACGGCAACGCCG-3′), used to change His445 to Asn; and H462N (5′-GCAAACGGCTAATACGACGAATCCG-3′), used to change His462 to Asn. All mutations were confirmed by DNA sequence analysis. The mutant *pgm* genes were subcloned and transformed into the appropriate *E.coli* expression strain as described. All mutant PGMs were overexpressed and purified through the heat treatment step as described (Chander *et al*., 1999) and they were all found to be full-length soluble proteins.

Biochemical analysis of mutant proteins

Divalent cations were removed from partially purified enzymes by passage through Chelex columns and incubation with EDTA as previously described (Chander *et al*., 1998), except that the proteins were incubated with 750 μM EDTA at 37°C for 6 h after passage through Chelex. PGM activity was measured using the two-step PGM assay described previously (Chander *et al.*, 1998). The concentration of Mn and the pH were varied in the first step of this assay in which 3PGA is converted to 2PGA. This step was carried out for 1 min at 65°C because of the high temperature optimum of the *B.stearothermophilus* PGM, and the concentration of 3PGA was 10 mM, which is at least 2-fold higher than the enzyme's K_m for 3PGA (Chander *et al*., 1999). In the second step of the two-step PGM assay, the 2PGA formed in the first step was quantitated by its generation of NADH via the enzymes enolase, pyruvate kinase and lactate dehydrogenase.

Structure determination

The cloning, production, purification, crystallization and preliminary X-ray diffraction analysis for both methionyl and selenomethionyl iPGM from *B.stearothermophilus* have been reported previously (Chander *et al*., 1999). The structure was solved using the multiwavelength anomalous dispersion (MAD) method (Table I). The positions of Se atoms in the selenomethionyl enzyme and the resulting phases were obtained using the automatic protocol of SOLVE (Terwilliger and Berendzen, 1999). All nine selenomethionyl atoms were identified unambiguously and the resulting electron density map was subjected to density modification procedures such as solvent flattening, histogram matching and multi-resolution scaling using the CCP4 suite of programs (CCP4, 1994). The electron density map was then traced using automated fitting procedures of ARP/wARP (Lamzin and Wilson, 1993). The polypeptide side chains were also automatically fitted with a confidence level of >85%. After manual inspection and evaluation and adjustments to the model, the structure was refined using X-PLOR least-squares procedures (Brunger, 1991), and the initial R_{cryst} and R_{free} were 0.35 and 0.40, respectively. The $|2F_o - F_c|$ and $|F_o - F_c|$ maps were calculated, the geometry of the structure was examined using a Ramachandran plot (Laskowski *et al*., 1993) and the model was corrected manually. The bulk solvent correction and the overall *B*-factor corrections were applied to the data during the subsequent structure refinement. The simulated annealing omit maps were also calculated in particular to correct the geometry about the region Asn274–Val302 and to determine the correct orientation of the

substrate in the active site. Simulated annealing refinement procedures were finally applied using the X-PLOR protocol (Brunger, 1991). The Mn^{2+} ions were located between the two domains using an $|F_o - F_c|$ electron density map with 6σ cutoff. The model was then subjected to individual *B*-factor refinements. The water molecules were fitted into an $|F_o - F_c|$ density map contoured at 3σ level using standard geometric criteria. The final R_{cryst} was 20.7% and the R_{free} was 24.7% (Table I). The stereochemistry of the structure is well defined with >89% of the residues in the core region of the Ramachandran plot. The only residue that lies outside of this core region but still in the energetically allowed area of the plot is Met374, which is between two turns of a surface-exposed loop. The electron density for this residue is good. Figures were drawn with Ribbons (Carson, 1987) or MolScript (Esnouf, 1997).

Modeling of the iPGM structure with 2PGA and Mn^{2+} ions

The refined crystal structure of iPGM with 3PGA and two Mn^{2+} ions was used as the reference for modeling of the structure with 2PGA. The 2PGA molecule was built based on standard geometric criteria and the structure of the 3PGA molecule, and was placed in the iPGM active site with maximum geometric overlap with the 3PGA molecule. The phosphate and carboxylate groups of 2PGA were placed in essentially the same places as for 3PGA in our iPGM structure. The position of 2PGA was adjusted to accommodate the active site interactions with this substrate, in particular to preserve the bidentate interactions of the phosphate group with Arg261 and the carboxylate group with Arg264. Several cycles of energy refinement with a conjugate gradient minimization were then carried out using the X-PLOR protocol. The protein component, together with the Mn^{2+} ions, was initially fixed, then restrained, and finally the restraints were removed to allow for unrestrained protein, Mn^{2+} and 2PGA refinement together. During this refinement the interactions of the phosphate group with Mn1 and the bidentate interaction with Arg261 as well as the bidentate interaction of the carboxyl group with Arg264 were preserved. There was also no significant change in the positions of Mn^{2+} ions as well as their ligands. The only significant movements in the active site during this refinement were observed for residues His123, Asp154, Arg185, Arg261 and for the ordered water molecule, Wat17.

Accession code

The coordinates and structure factors have been deposited at the Brookhaven Protein Data Bank under the accession code 1EJJ.

Acknowledgements

The authors thank Dr A.Perrakis for his help with the ARP/wARP package. Diffraction data for this study were collected at Brookhaven National Laboratory in the Biology Department single-crystal diffraction facility at beamlines X12-C and X25-C in the National Synchrotron Light Source. This facility is supported by the United States Department of Energy Offices of Health and Environmental Research and of Basic Energy Sciences under prime contract DE-AC02-98CH10886, by the National Science Foundation, and by National Institutes of Health (NIH) Grant 1P41 RR12408-01A1. This work was supported by NIH grant GM19698 (P.S.) and a high-resolution structure supplement to this grant (P.S. and M.J.J.).

References

Bazan,J.F. and Fletterrick,R.J. (1990) Tertiary structure modeling of 6-phosphofructo-2-kinase/fructose-2,6-bisphosphatase: structural, functional and evolutionary design of a bifunctional enzyme. In Pilkis,S.J. (ed.), *Fructose 2,6-Bisphosphate*. CRC Press, Boca Raton, FL, pp. 125–171.

Blatter,A.W. and Knowles,J.R. (1980) Phosphoglycerate mutases: stereochemical course of the phosphoryl group transfers catalyzed by the cofactor-dependent enzyme from rabbit muscle and the cofactor-independent enzyme from wheat germ. *Biochemistry*, **19**, 738–743.

Breathnach,R. and Knowles,J.R. (1977) Phosphoglycerate mutase from wheat germ: studies with ^{18}O-labeled substrate, investigations of the phosphatase and phosphoryl transfer activities and evidence for a phosphoryl–enzyme intermediate. *Biochemistry*, **16**, 3054–3060.

Britton,H.G., Carrerras,J. and Grisolia,S. (1971) Mechanism of action of 2,3-diphosphoglycerate-independent phosphoglycerate mutase. *Biochemistry*, **10**, 4522–4533.

Brunger,A.T. (1991) *X-PLOR*: *A System for Crystallography and NMR*. Yale University Press, New Haven, CT.

Campbell,J.W., Watson,H.C. and Hodgson,G.I. (1974) Structure of yeast phosphoglycerate mutase. *Nature*, **250**, 301–303.

Carreras,J., Mezquita,J., Bosch,J., Bartrons,R. and Pons,G. (1982) Phylogeny and ontogeny of the phosphoglycerate mutases—IV. Distribution of glycerate-2,3-P2 dependent and independent phosphoglycerate mutases in algae, fungi, plants and animals. *Comp. Biochem. Physiol. B*, **71**, 591–597.

Carson,M.J. (1987) Ribbon models of macromolecules. *J. Mol. Graph.*, **5**, 103–106.

Chander,M., Setlow,B. and Setlow,P. (1998) The enzymatic activity of phosphoglycerate mutase from gram-positive endospore-forming bacteria requires Mn^{2+} and is pH sensitive. *Can. J. Microbiol.*, **44**, 759–767.

Chander,M., Setlow,P., Lamani,E. and Jedrzejas,M.J. (1999) Structural studies on a 2,3-diphosphoglycerate independent phosphoglycerate mutase from *Bacillus stearothermophilus*. *J. Struct. Biol.*, **126**, 156–165.

Collaborative Computational Project, Number 4 (1994) The CCP4 suite: programs for protein crystallography. *Acta Crystallogr. D*, **50**, 760–763.

Esnouf,R.M. (1997) An extensively modified version of MolScript that includes greatly enhanced coloring capabilities. *J. Mol. Graph.*, **15**, 133–138.

Fothergill-Gilmore,L.A. and Watson,H.C. (1989) The phosphoglycerate mutases. *Adv. Enzymol. Relat. Areas Mol. Biol.*, **62**, 227–313.

Fraser,H.I., Kratskhelia,M. and White,M.F. (1999) The two analogous phosphoglycerate mutases of *Escherichia coli*. *FEBS Lett.*, **455**, 344–348.

Galperin,M.Y., Bairoch,A. and Koonin,E.V. (1998) A superfamily of metalloenzymes unifies phosphopentomutase and cofactor-independent phosphoglycerate mutase with alkaline phosphatases and sulfatases. *Protein Sci.*, **7**, 1829–1835.

Gatehouse,J.A. and Knowles,J.R. (1977) Phosphoglycerate mutase from wheat germ: studies with isotopically labeled 3-phospho-D-glycerates showing that the catalyzed reaction is intramolecular. *Biochemistry*, **16**, 3045–3050.

Grana,X., Lecea,L., El-Maghrabi,M.R., Urena,J.M., Caellas,C., Carreras,J., Puigdomenech,P., Pilkis,S.J. and Climent,F. (1992) Cloning and sequencing of a cDNA encoding 2,3-bisphosphoglycerate-independent phosphoglycerate mutase from maize. *J. Biol. Chem.*, **267**, 12797–12803.

Harding,M.M. (1999) The geometry of metal–ligand interactions relevant to proteins. *Acta Crystallogr. D*, **55**, 1432–1443.

Holm,L. and Sander,C. (1994) Searching protein structure data bases has come of age. *Proteins*, **19**, 165–173.

Huang,Y. and Dennis,D.T. (1995) Histidine residues 139, 363 and 500 are essential for catalytic activity of cofactor-independent phosphoglyceromutase from developing endosperm of the castor plant. *Eur. J. Biochem.*, **229**, 395–402.

Johnson,M. and Price,N.C. (1988) Do metal ions promote the re-activation of the 2,3-bisphosphoglycerate-independent phosphoglycerate mutases? *Biochem. J.*, **252**, 111–117.

Kanyo,Z.F., Scolnick,L.R., Ash,D.E. and Christianson,D.W. (1996) Structure of a unique binuclear manganese cluster in arginase. *Nature*, **383**, 554–557.

Kuhn,N.J., Talbot,J. and Ward,S. (1991) pH-sensitive control of arginase by Mn(II) ions at submicromolar concentrations. *Arch. Biochem. Biophys.*, **286**, 217–221.

Kuhn,N.J., Setlow,B., Setlow,P., Cammack,R. and Williams,R. (1995) Cooperative manganese(II) activation of 3-phosphoglycerate mutase of *Bacillus megaterium*. A biological pH-sensing mechanism in bacterial spore formation and germination. *Arch. Biochem. Biophys.*, **320**, 35–42.

Lamzin,V.S. and Wilson,K.S. (1993) Automated refinement of protein models. *Acta Crystallogr. D*, **49**, 129–147.

Laskowski,R., Macarthur,M., Moss,D. and Thornton,J. (1993) PROCHECK: a program to check the stereochemical qualities of protein structures. *J. Appl. Crystallogr.*, **26**, 283–290.

Magill,N.G., Cowan,A.E., Koppel,D.E. and Setlow,P. (1994) The internal pH of the forespore compartment of *Bacillus megaterium* decreases by about 1 pH unit during sporulation. *J. Bacteriol.*, **178**, 2252–2258.

Magill,N.G., Cowan,A.E., Leyva-Vazquez,M.A., Brown,M., Koppel,D.E. and Setlow,P. (1996) Analysis of the relationship between the decrease in pH and accumulation of 3-phosphoglyceric acid in developing forespores of *Bacillus* species. *J. Bacteriol.*, **178**, 2204–2210.

Monder,C. (1965) Metal ion interactions and glutamine synthetase activity. *Biochemistry*, **4**, 2677–2686.

Nairn,J.N., Krell,T., Coggins,J.R., Pitt,A.R., Fothergill-Gilmore,L.A., Walter,R. and Price,N.N. (1995) The use of mass spectrometry to examine the phosphorylation and hydrolysis of the phosphorylated form of phosphoglycerate mutase. *FEBS Lett.*, **359**, 192–194.

Rigden,D.J., Alexeev,D., Phillips,S.E.V. and Fothergill-Gilmore,L.A. (1998) The 2.3 Å X-ray crystal structure of *S.cerevisiae* phosphoglycerate mutase. *J. Mol. Biol.*, **276**, 449–459.

Rose,Z.B. (1971) The phosphorylation of yeast phosphoglycerate mutase. *Arch. Biochem. Biophys.*, **146**, 359–360.

Schneider,G., Lindqvist,Y. and Vihko,P. (1993) Three-dimensional structure of rat acid phosphatase. *EMBO J.*, **12**, 2609–2615.

Singh,R.P. and Setlow,P. (1979) Purification and properties of phosphoglycerate phosphomutase from spores and cells of *Bacillus megaterium. J. Bacteriol.*, **137**, 1024–1027.

Smith,G.C., McWilliams,A.D. and Hans,L.F. (1988) Wheat germ phosphoglycerate mutase. Evidence for a metalloenzyme. *Biochem. Biophys. Res. Commun.*, **136**, 336–340.

Sofia,H.J., Burland,V., Daniels,D.L., Plunkett,G.,III and Blatter,F.R. (1994) Analysis of the *Escherichia coli* genome. V. DNA sequence of the region from 76.0 to 81.5 minutes. *Nucleic Acids Res.*, **22**, 2576–2586.

Sowadski,J.M., Handschumacher,M.D., Murthy,M.H.K., Foster,B.A. and Wyckoff,H.W. (1985) Refined structure of alkaline phosphatase from *Escherichia coli* at 2.8 Å resolution. *J. Mol. Biol.*, **186**, 417–433.

Stec,B., Hehir,M.J., Brennan,C., Nolte,M. and Kantrowitz,E.R. (1998) Kinetic and X-ray structure studies of three mutant *E.coli* alkaline phosphatases: insights into the catalytic mechanism without the nucleophile Ser102. *J. Mol. Biol.*, **277**, 647–662.

Sternberg,M.J.E., Cohen,F.E., Taylor,W.R. and Feldmann,R.J. (1981) Analysis and prediction of structural motifs in the glycolytic enzymes. *Philos. Trans. R. Soc. Lond. B*, **293**, 177–189.

Terwilliger,T.C. and Berendzen,J. (1999) Automated MAD and MIR structure solution. *Acta Crystallogr. D*, **55**, 849–861.

Watabe,K. and Freese,E. (1979) Purification and properties of the manganese-dependent phosphoglycerate mutase of *Bacillus subtilis. J. Bacteriol.*, **137**, 773–778.

White,M.F. and Fothergill-Gilmore,L.A. (1992) Development of a mutagenesis, expression and purification system for yeast phosphoglycerate mutase. *Eur. J. Biochem.*, **207**, 709–714.

White,M.F., Fothergill-Gilmore,L.A., Kelly,S.M. and Price,N.C. (1993) Substitution of His-181 by alanine in yeast phosphoglycerate mutase leads to cofactor-induced dissociation of the tetrameric structure. *Biochem. J.*, **291**, 479–483.

Received January 4, 2000; revised and accepted February 7, 2000